Inorganic Chemistry

Article

pubs.acs.org/IC

Synthesis, Electrochemistry, and Single-Molecule Conductance of Bimetallic 2,3,5,6-Tetra(pyridine-2-yl)pyrazine-Based Complexes

Ross Davidson,[†] Jing-Hong Liang,[‡,§] David Costa Milan,[‡] Bing-Wei Mao,[§] Richard J. Nichols,[‡] Simon J. Higgins,[‡] Dmitry S. Yufit,[†] Andrew Beeby,[†] and Paul J. Low*[,∥]

[†]Department of Chemistry, Durham University, South Road, Durham DH1 3LE, U.K.

[‡]Department of Chemistry, University of Liverpool, Crown Street, Liverpool L69 7ZD, U.K.

[§]State Key Laboratory of Physical Chemistry of Solid Surfaces and College of Chemistry and Chemical Engineering, Xiamen University, Xiamen 361005, Fujian, China

[∥]School of Chemistry and Biochemistry, University of Western Australia, 35 Stirling Highway, Perth, Western Australia 6009, Australia

Supporting Information

ABSTRACT: The ligands 4′-(4-(methylthio)phenyl)-2,2′:6′,2″-terpyridine ($\mathbf{L^1}$), 4′-((4-(methylthio)phenyl)-ethynyl)- 2,2′:6′,2″-terpyridine ($\mathbf{L^2}$), and bis(tridentate) bridging ligand 2,3,5,6-tetra(pyridine-2-yl)pyrazine (tpp) were used to prepare the complexes $[Ru(\mathbf{L^1})_2][PF_6]_2$ ($[\mathbf{1}][PF_6]_2$, $[Ru(\mathbf{L^2})_2][PF_6]_2$ ($[\mathbf{2}][PF_6]_2$), $[\{(\mathbf{L^1})Ru\}(\mu\text{-tpp})\{Ru(\mathbf{L^1})\}][PF_6]_4$ ($[\mathbf{3}][PF_6]_4$), and $[\{(\mathbf{L^2})Ru\}(\mu\text{-tpp})\{Ru(\mathbf{L^2})\}][PF_6]_4$ ($[\mathbf{4}][PF_6]_4$). Crystallographically determined structures give S···S distances of up to 32.0 Å in $[\mathbf{4}]^{4+}$. On the basis of electrochemical estimates, the highest occupied molecular orbitals of these complexes fall between −5.55 and −5.85 eV, close to the work function of clean gold (5.1−5.3 eV). The decay of conductance with molecular length across this series of molecules is approximately exponential, giving rise to a decay constant (pseudo β-value) of 1.5 nm^{-1}, falling between decay factors for oligoynes and oligophenylenes. The results are consistent with a tunnelling mechanism for the single-molecule conductance behavior.

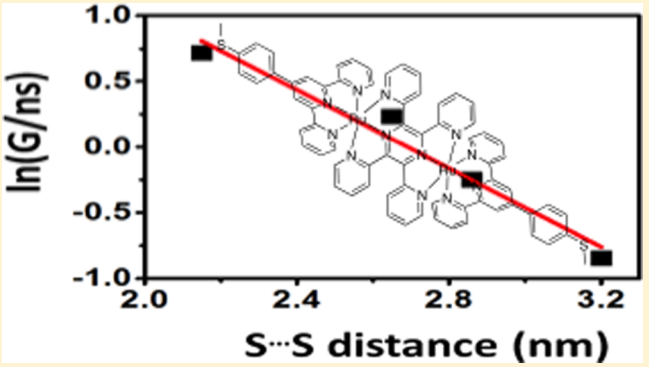

INTRODUCTION

With the increased availability of scanning tunneling microscopy (STM) and break-junction technology great strides have been made in the understanding of single-molecule conductance,[1] particularly with regard to pure organic compounds such as polyynes,[2,3] oligophenylenes,[4] and oligoaryleneethynylenes.[5] More recently, attention has been turned to the role that metal centers and complexes may play when incorporated into the backbone of a wirelike molecule.[6−10] These metal complexes are of a special interest in the realm of molecular electronics, as they hold the potential for finer tuning of the molecular orbitals to match the Fermi levels of the electrodes, and also the possibilities to augment electronic characteristics through accessing available redox levels,[11] electrochemical gating,[12,13] redox or optical switching,[14] and magnetic effects,[15] as well as high thermoelectric efficiency.[16]

Metal complexes based on 2,2′:6′,2″-terpyridine (tpy) ligands have proven to be valuable for evaluation of many of these features of metal complexes in molecular electronics, and to-date these are some of the most studied metal complexes to be incorporated into a metallmoleculelmetal junction and related moleculelmetal assemblies.[11,12,17−25] The $\{M(tpy)_2\}^{n+}$ structural element has proven particularly popular being easily accessed synthetically and functionalized to give linear molecular geometries,[26] featuring a wide range of metal ions, allowing a selection of physical and chemical properties relating the charge, size, and redox and magnetic properties of the complex to be readily examined. The 2,3,5,6-tetra(pyridine-2-yl)pyrazine (tpp) ligand, which may be regarded as a "back-to-back" fused bis-tpy ligand, is a valuable structural element when seeking to figuratively and literally extend these studies. The tpp ligand, used in conjugation with tpy coligands, provides a convenient entry point to linear, multimetallic assemblies in which the metal centers can be strongly coupled,[27−31] and it is well-suited to use in the construction of molecular arrays both in solution and from "on-surface" coordination chemistry approaches.[20,21]

We now report the synthesis, electrochemical properties, and single-molecule conductance behavior of mono and bimetallic ruthenium complexes based on $[Ru(tpy)_2]^{2+}$ and $[\{(tpy)Ru\}(\mu\text{-tpp})\{Ru(tpy)\}]^{4+}$ structural motifs. The multimetallic

Received: March 8, 2015
Published: May 14, 2015

DOI: 10.1021/acs.inorgchem.5b00507
Inorg. Chem. 2015, 54, 5487−5494

complexes are shown to be capable of serving as wirelike assemblies of up to 3 nm long.

EXPERIMENTAL SECTION

General Details. Microwave reactions were performed in a Biotage Microwave Synthesizer (model Initiator 2.5). NMR spectra were recorded in deuterated solvent solutions on Bruker DRX-400 and Varian Inova 300, 400, and 500 spectrometers and referenced against solvent resonances (^{1}H, ^{13}C). Electrospray mass spectra (ESMS) were recorded on a TQD mass spectrometer (Waters Ltd., U.K.) in acetonitrile. Atmospheric solids analysis probe mass spectra (ASAP-MS) were collected on a LCT Premier XE mass spectrometer (Waters Ltd., U.K.) in dichloromethane. Microanalyses were performed by Elemental Analysis Service, London Metropolitan University, U.K. Electrochemical analyses of the complexes were performed using a PalmSens EmStat^2 potentiometer, with platinum working, platinum counter, and platinum pseudo reference electrodes, from solutions in acetonitrile containing 0.1 M supporting electrolyte (tetrabutylammonium hexafluorophosphate, NBu_4PF_6), scan rate = 100 mV s^{-1}. The ferrocene/ferrocinium couple was used as the internal reference.

Analytical grades of solvents were used. The compounds 4′-(((trifluoromethyl)sulfonyl)oxy)-2,2′:6′,2″-terpyridine (tpyOTf),[32] 4-ethynylthioanisole ($MeSC_6H_4C{\equiv}CH$),[33] 4′-(4-(methylthio)phenyl)-2,2′:6′,2″-terpyridine ($\mathbf{L^1}$),[34] $[Ru(\mathbf{L^1})_2][PF_6]_2$ ($[\mathbf{1}][PF_6]_2$),[34] and $\{Cl_3Ru\}(\mu\text{-tpp})\{RuCl_3\}$[35] were synthesized according to literature methods. All other chemicals were sourced from standard suppliers. Hydrated ruthenium chloride, $RuCl_3{\cdot}nH_2O$, was assumed to be of approximate composition $RuCl_3{\cdot}3H_2O$.

Synthesis. *4′-((4-(Methylthio)phenyl)ethynyl)-2,2′:6′,2″-terpyridine ($\mathbf{L^2}$).* Triethylamine (NEt_3, 7 mL) was added to a solution containing tpyOTf (250 mg, 0.65 mmol) and $MeSC_6H_4C{\equiv}CH$ (96 mg, 0.65 mmol) in tetrahydrofuran (THF, 20 mL). The solution was freeze−pump−thawed three times before $Pd(PPh_3)_4$ (75 mg, 0.065 mmol) was added. The solution was refluxed overnight in the dark, after which time the solvent was removed. The solid residue was extracted in dichloromethane and filtered. The filtrate was passed down a silica column initially with neat CH_2Cl_2 then CH_2Cl_2/acetonitrile (1:1) to elute the product. The main fraction was collected, dried, and washed with methanol to remove the remaining impurities, giving a white solid. Crystals were grown via the slow evaporation of a hexane/dichloromethane solution. Yield: 193 mg (78%). ASAP-MS: 380 m/z $[MH]^+$. ^{1}H NMR ($CDCl_3$): δ 8.70 (d (J^1_{HH} = 5 Hz), 2H), 8.60 (d (7), 2H), 8.53 (s, 2H), 7.85 (t (7), 2H), 7.44 (d (7), 2H), 7.33 (t (7), 2H), 7.20 (d (7), 2H), 2.48 (s, 3H) ppm. ^{13}C{^{1}H} NMR ($CDCl_3$): δ. 155.5, 155.3, 149.3, 140.5, 137.0, 133.5, 132.1, 125.7, 124.0, 122.7, 121.2, 118.5, 93.8, 87.5, 15.2 ppm. Anal. Calc. for $C_{24}H_{17}N_3S$: C, 75.96; H, 4.52; N, 11.07%. Found: C, 75.86; H, 4.45; N, 11.02%.

$[Ru(\mathbf{L^2})_2][PF_6]_2$ $[\mathbf{2}][PF_6]_2$. The ligand $\mathbf{L^2}$ (100 mg, 0.26 mmol) and $RuCl_3{\cdot}3H_2O$ (34 mg, 0.13 mmol) were added to ethylene glycol (4 mL). The resulting suspension was degassed by bubbling nitrogen through it before being heated by microwave to 160 °C for 30 min. The red solution was poured into an aqueous, saturated KPF_6 solution, forming a red precipitate. The precipitate was collected by filtration, washed thoroughly with water, and air-dried. The red solid was extracted in acetone and filtered, and the filtrate was taken to dryness, leaving a red residue. This residue was dissolved in the minimum volume of CH_2Cl_2 and purified by elution through a neutral alumina column with an acetonitrile/CH_2Cl_2 (1:1). The orange band was collected, and the solvent was removed, leaving the title product. Crystals were grown by vapor diffusion of diethyl ether into an acetonitrile solution. Yield: 119 mg (80%). ESMS: 430 m/z $[M]^{2+}$. ^{1}H NMR($CDCl_3$): δ 8.87 (s, 4H), 8.52 (d (J^1_{HH} = 8 Hz), 4H), 7.96 (t (8), 4H), 7.71 (d (8), 4H), 7.44−7.42 (m, 8H), 7.20 (t (7), 4H), 2.59 (s, 6H) ppm. ^{13}C{^{1}H} NMR ($CDCl_3$): δ. 157.5, 155.1, 152.6, 142.6, 138.2, 132.4, 130.5, 127.6, 125.7, 125.1, 124.5, 117.0, 97.11, 86.3, 14.0 ppm. Anal. Calc. for $C_{48}H_{34}F_{12}N_6P_2RuS_2$: C, 50.13; H, 2.98; N, 7.31%. Found: C, 50.00; H, 3.00; N, 7.31%.

$[\{(\mathbf{L^1})Ru\}(\mu\text{-tpp})\{Ru(\mathbf{L^1})\}][PF_6]_4$ $[\mathbf{3}][PF_6]_4$. The compounds $\mathbf{L^1}$ (128 mg, 0.36 mmol) and $\{Cl_3Ru\}(\mu\text{-tpp})\{RuCl_3\}$ (100 mg, 0.12 mmol) were added to ethylene glycol (4 mL). This suspension was degassed by bubbling nitrogen through it before being heated by microwave to 160 °C for 30 min. The purple solution was poured into an aqueous saturated KPF_6 solution, forming a purple precipitate. The precipitate was collected by filtration, washed thoroughly with water, and air-dried. The purple solid was washed from the frit with acetone, the filtrate was collected, and solvent was removed, leaving a purple residue. This was eluted down a neutral alumina column with acetonitrile/CH_2Cl_2 (1:1) collecting the purple band; the solvent was removed leaving the title product. Crystals were grown by vapor diffusion of diethyl ether into an acetonitrile solution. Yield: 97 mg (43%). ESMS: 325 m/z $[M]^{4+}$. ^{1}H NMR($CDCl_3$): δ 9.15 (s, 4H), 8.99 (d (J^1_{HH} = 8 Hz), 4H), 8.79 (d (8), 4H), 8.26 (d (8), 4H), 8.10 (t (7), 4H), 7.95 (t (8), 4H), 7.85 (d (6), 4H), 7.76 (d (6), 4H), 7.70 (d (7), 4H), 7.45 (t (7), 4H), 7.32 (t (7), 4H), 2.70 (s, 6H) ppm. ^{13}C{^{1}H} NMR ($CDCl_3$): δ. 157.8, 155.0, 154.7, 154.0, 153.1, 149.8, 149.3, 143.3, 139.0, 137.8, 132.3, 129.4, 129.2, 128.2, 127.6, 126.4, 125.0, 121.7, 14.2 ppm. Anal. Calc. for $C_{68}H_{50}F_{24}N_{12}P_4Ru_2S_2$: C, 43.41; H, 2.68; N, 8.93%. Found: C, 43.50; H, 2.84; N, 8.91%.

$[\{(\mathbf{L^2})Ru\}(\mu\text{-tpp})\{Ru(\mathbf{L^2})\}][PF_6]_4$ $[\mathbf{4}][PF_6]_4$. The compound was prepared using the same procedure as that described for $[\mathbf{3}][PF_6]_4$, except $\mathbf{L^2}$ was used in place of $\mathbf{L^1}$. Yield: 106 mg (46%). ESMS: 337 m/z $[M]^{4+}$. ^{1}H NMR($CDCl_3$): 9.03 (s, 4H), 9.00 (d (J^1_{HH} = 8 Hz), 4H), 8.67 (d (8), 4H), 8.11 (t (8), 4H), 7.97 (t (8), 4H), 7.83 (d (6), 4H), 7.78−7.76 (m, 8H), 7.48−7.45 (m, 8H), 7.36 (t (6), 4H), 2.62 (s, 6H) ppm. ^{13}C{^{1}H} NMR ($CDCl_3$): δ. 157.1, 154.8, 154.7, 154.0, 153.3, 142.9, 139.1, 137.9, 132.6, 132.5, 129.5, 129.3, 127.9, 127.4, 125.7, 125.0, 116.8, 98.1, 86.2, 14.0 ppm. Anal. Calc. for $C_{72}H_{50}F_{24}N_{12}P_4Ru_2S_2{\cdot}4H_2O$: C, 43.21; H, 2.92; N, 8.40%. Found: C, 43.21; H, 2.57; N, 8.72%.

Single-Molecule Conductance Measurements. Gold-on-glass substrates (Arrandee, Schröer, Germany) were rinsed with acetone and then flame-annealed with a butane torch until the slide glowed with a very slight orange hue. The slide was retained in this state for ∼20 s during which time the torch was kept in motion across the sample to avoid deleterious overheating. This procedure was performed three times to generate extended Au (111) terraces, as seen by STM imaging. The freshly annealed substrates were immersed in a 1×10^{-4} M acetonitrile (99.9% Chromasolv Plus for HPLC) solution of the complex under investigation for 1 min, after which time the gold sample was removed, washed with ethanol, and then dried in a flow of argon. The short immersion time and low concentration of solution were chosen to promote low molecular coverage of the gold surface, which favor the formation of single molecule over multimolecular junctions.

Conductance values of those compounds and the break-off distance were obtained with an STM (Agilent 5500 SPM microscope), using the $I(s)$ technique.[36,37] In this method an electrochemically etched gold tip is approached close to the substrate surface and then retracted with the tunnelling current (I) recorded against distance (s). In the case where molecular junctions are formed, significant deviations from the usual exponential decay of current are observed, with marked current plateaus and steps appearing as the tip was retracted. The step is seen as the tip is retracted beyond the maximal stretched length of the junction, with the molecular bridge breaking, which leads to the sharp decrease in current and the observed steplike feature. The resulting $I(s)$ curves are binned in current divisions (0.025 nS) and plotted to give a conductance histogram comprised of hundreds of scans that show plateaus synonymous with molecular junction formation.

X-ray Crystallography. The single-crystal X-ray data for all compounds were collected at 120.0(2) K on a Bruker D8Venture 3-circle diffractometer (Photon100 CMOS detector, IμS microsource, focusing mirrors, λMo Kα, λ = 0.710 73 Å) equipped with Cryostream (Oxford Cryosystems) open-flow nitrogen cryostat. Following multiscan absorption corrections and solution by direct methods, the structures were refined against F^2 with full-matrix least-squares using the SHELXTL[38] and OLEX2[39] software. Anisotropic displacement

DOI: 10.1021/acs.inorgchem.5b00507
Inorg. Chem. 2015, 54, 5487−5494

parameters were employed for the nondisordered non-hydrogen atoms. Disordered atoms in the structure $[2][PF_6]_2$ were refined isotropically with fixed with fixed site occupancy factor (SOF) = 0.5 for $[PF_6]^-$ anion and 0.4:0.6 for terminal Me-group. All H atoms were added at calculated positions and refined by use of riding models with isotropic displacement parameters based on those of the parent atom. The structures $[2][PF_6]_2$ and $[4][PF_6]_4$ alongside with well-determined acetonitrile solvent molecules contain some severely disordered solvent molecules, which could not be identified and refined. Their contribution to the structural factors was taken into account by applying the MASK procedure of the OLEX2 program package (40 and 13 e for the structures $[2][PF_6]_2$ and $[4][PF_6]_4$, respectively). The crystallographic and refinement parameters are listed in Supporting Information. Crystallographic data for the structures were deposited with the Cambridge Crystallographic Data Centre as supplementary publication CCDC-1050880−1050882.

Computational Studies. All the calculations were performed with the Gaussian 09 program package,[40] using the B3LYP functional.[41,42] A comparison was made between models using SDD basis set for all atoms or LANL2DZ basis set for Ru and 6-31G(d) for all other atoms.[43,44] On the basis of agreement with the crystallographic data, the LANL2DZ/6-31G(d) basis set was chosen.

RESULTS AND DISCUSSION

Synthesis. The elementary design of compounds for single-molecule conductance studies within an STM-based metall molecule|metal junction calls for a linear or pseudo linear molecular fragment terminated by suitable surface binding groups at each end of the molecule.[37] Here, the thiomethyl (-SMe) moiety was chosen as the surface contacting or anchoring group,[45,46] allowing for good contact to gold substrates and the STM tip and compatibility with subsequent synthetic steps, without the additional complications of the protecting group strategies involved in the use of thiolates.[47] The parent ligand, 4′-(4-(methylthio)phenyl)-2,2′:6′,2″-terpyridine ($\mathbf{L^1}$) bearing the SMe moiety was synthesized by the previously reported route involving a Kröhnke condensation of 2-acetylpyridine with 4-(methylthio)benzaldehyde (Scheme 1).[34] The new, extended ligand $\mathbf{L^2}$ was synthesized by cross-coupling of tpyOTf with the 4-ethynylthioanisole ($MeSC_6H_4C{\equiv}CH$) in an analogous fashion to that described elsewhere for other 4-ethynyl-substituted terpyridines (Scheme 2).[48−50]

For reference purposes, the homoleptic mononuclear complexes $[1][PF_6]_2$ and $[2][PF_6]_2$ were prepared from reactions of $RuCl_3{\cdot}3H_2O$ with $\mathbf{L^1}$ (Scheme 1) and $\mathbf{L^2}$ (Scheme 2), respectively. The compound $[1][PF_6]_2$ was prepared by the literature method as described by Constable et al. from the reaction of $\mathbf{L^1}$ and $RuCl_3{\cdot}3H_2O$ in refluxing methanol with a promoting amine (e.g., ethyl morpholine),[51] followed by filtration and precipitation with the addition of NH_4PF_6 (method *i*, Scheme 1).[34] For $[2][PF_6]_2$ both this approach (method *i*) and an alternative procedure involving microwave heating of a suspension of $RuCl_3{\cdot}3H_2O$ and $\mathbf{L^2}$ in ethylene glycol, followed by precipitation into aqueous KPF_6 (method *ii*) were explored. In this instance both methods gave similar yields, method *ii* being favored in this report for its greater convenience (Scheme 2).

The analogous bimetallic complexes $[3][PF_6]_4$ and $[4][PF_6]_4$ were targeted through combination of the terminal ligands $\mathbf{L^1}$ and $\mathbf{L^2}$ with the bis(tridentate) bridging ligand 2,3,5,6-tetra(pyridine-2-yl)pyrazine (tpp) (Scheme 1, Scheme 2). Reaction of $RuCl_3(\mathbf{L^1})$[34] with tpp under either conventional or microwave heating gave only the polymeric complex of ruthenium and tpp. Similarly, conventional heating of an excess

Scheme 1. Synthetic Scheme for $\mathbf{L^1}$, $[1][PF_6]_2$, and $[3][PF_6]_4$[a]

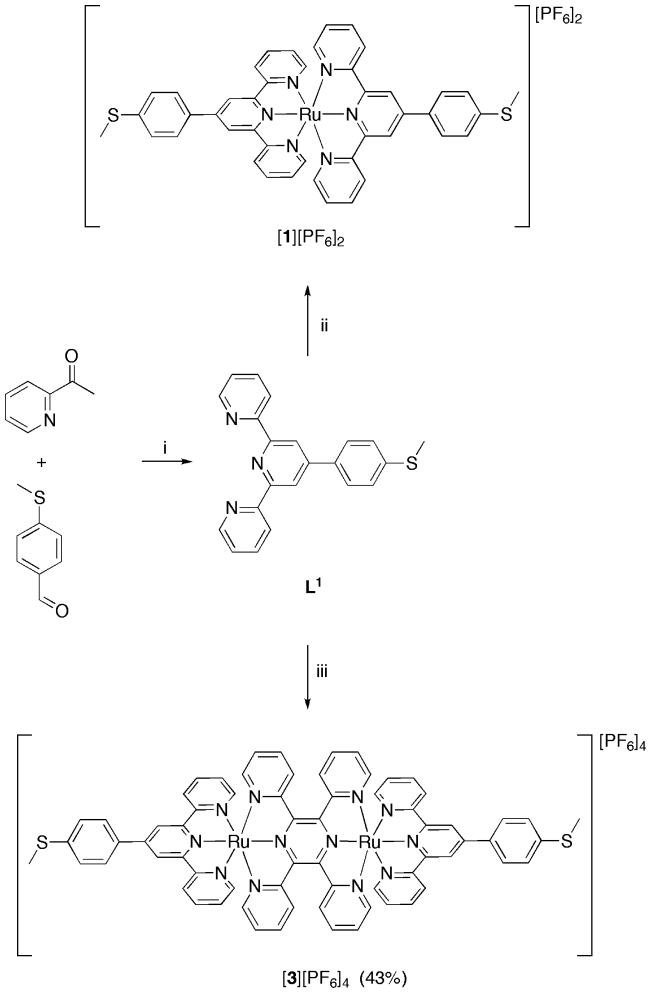

[a](i) EtOH and NH_4Ac. (ii) (a) $RuCl_3{\cdot}3H_2O$, methanol, ethyl morpholine. (b) NH_4PF_6. (iii) (a) $\{Cl_3Ru\}(\mu\text{-tpp})\{RuCl_3\}$, ethylene glycol, microwave, 160°C, 30 min. (b) KPF_6.

of either $\mathbf{L^1}$ or $\mathbf{L^2}$ with the biruthenium trichloride complex $\{Cl_3Ru\}(\mu\text{-tpp})\{RuCl_3\}$[35] also gave ruthenium-tpp polymer, presumably as a result of competing decomplexation/coordination processes. However, under microwave heating, from $\{Cl_3Ru\}(\mu\text{-tpp})\{RuCl_3\}$ and either $\mathbf{L^1}$ or $\mathbf{L^2}$ a mixture consisting of the desired bimetallic products with small amounts of the homoleptic tpy complexes was formed. These bi- and mononuclear complexes were readily separated chromatographically, providing a convenient route to $[3][PF_6]_4$ (43%) and $[4][PF_6]_4$ (46%).

Molecular Structures. The structure $\mathbf{L^2}$ contains two virtually identical crystallographically independent molecules A and B (one of the molecules is shown in Figure 1), with selected bond lengths and angles given in Supporting Information. The structure shows the 4-ethynylthioanisole attached to the terpyridine (tpy) motif at the 4′-position, confirming the assignment by NMR spectroscopy and mass spectrometry. The three pyridine rings are almost coplanar. The nitrogen atoms on the external pyridine rings are directed so as to maximise intramolecular hydrogen bonding. The phenylene ring (C18−C21) is rotated about the ethynyl bond

DOI: 10.1021/acs.inorgchem.5b00507
Inorg. Chem. 2015, 54, 5487−5494

Scheme 2. Synthetic Scheme for L^2, $[2][PF_6]_2$, and $[4][PF_6]_4$[a]

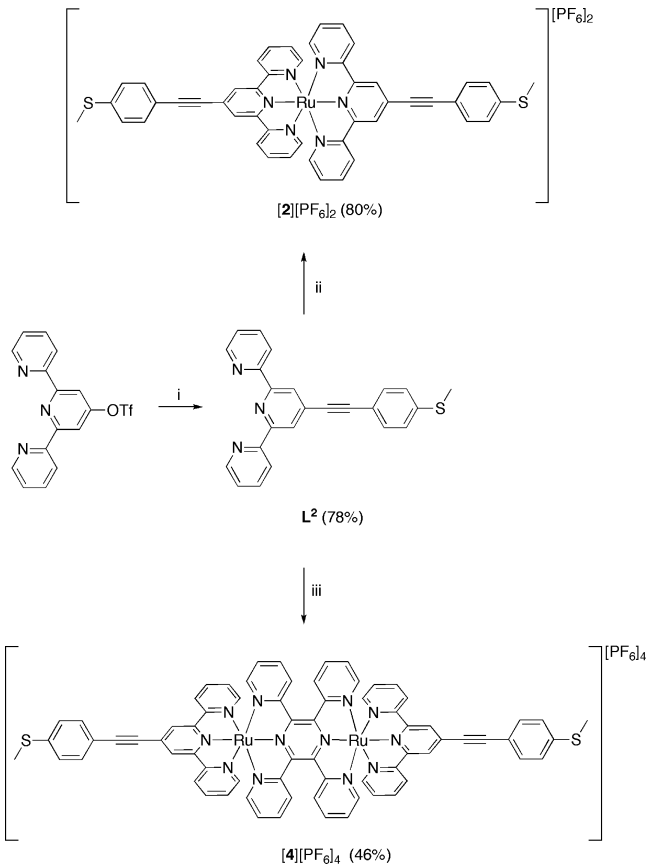

[a](i) $MeSC_6H_4C{\equiv}CH$, $Pd(PPh_3)_4$, NEt_3 and THF. (ii) (a) $RuCl_3{\cdot}3H_2O$, ethylene glycol, microwave, 160°C, 30 min. (b) KPF_6. (iii) (a) $\{Cl_3Ru\}(\mu\text{-tpp})\{RuCl_3\}$, ethylene glycol, microwave, 160°C, 30 min. (b) KPF_6.

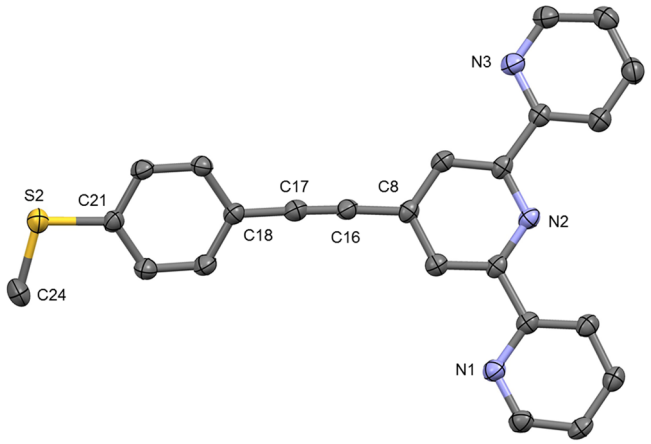

Figure 1. A plot of molecule A in the structure L^2, with hydrogen atoms omitted for clarity. Thermal ellispsoids are plotted at 50%.

relative to the tpy moiety by 21.6° (molecule A) and 24.3° (molecule B).

The cation in the structure $[2][PF_6]_2{\cdot}CH_3CN$ is shown in Figure 2, and selected bond lengths and angles are given in the Supporting Information. The structure shows the two L^2 ligands coordinated to the ruthenium center via the tpy units giving an octahedral "N_6" coordination sphere, confirming the assignment of the structure made by NMR spectroscopy and mass spectrometry. The axial Ru−N bond lengths are 1.967(3) (Ru1−N2) and 1.966(3) Å (Ru1−N5), similar to those of $[Ru(tpy)_2][PF_6]_2{\cdot}2CH_3CN$. The ethynyl-substituted phenylene groups are almost coplanar with the associated tpy fragments, although in the absence of any significant structural evidence for extensive delocalization, the orientation of this group is likely governed by packing forces. The alkyne bond lengths show no significant difference when the structures of the free ligand and complex are compared (C16−C17 = 1.180(6) Å, $[2]^{2+}$; 1.204(3) Å, L^2). Overall, this gives a S···S distance of ∼26.5 Å in $[2]^{2+}$, which is 4.9 Å longer than that in $[Ru(L^1)_2][PF_6]_2$.[34]

The bimetallic cation in the structure $[4][PF_6]_4{\cdot}3CH_3CN$ is shown in Figure 3; selected bond lengths and angles are given in the Supporting Information. The structure shows two ruthenium atoms coordinated by the phenazine ring of tpp and its peripheral pyridines. The "N_6" coordination sphere of the metals is completed by L^2. The tpp ligand displays the typical bending of the phenazine ring, resulting in a gracefully curved shape to the molecular tetracation. As with $[2][PF_6]_2$ the alkyne bond lengths remain unchanged from that of the ligand with C41−C40 = 1.198(12) and C64−C65 = 1.198(10) Å. The ruthenium−nitrogen bond lengths for $[4][PF_6]_4$ Ru1−N8 = 1.994(5) and Ru1−N1 = 1.975(5) Å are also similar to the comparable distances found in $[\{(tpy)Ru\}(\mu\text{-tpp})\{Ru(tpy)\}][PF_6]_4$ (1.96(2), 1.98(2) and 1.96(2), 2.00(2) Å)[53] and $[2][PF_6]_2{\cdot}CH_3CN$, suggesting that the electronic nature of the Ru-tpp-Ru remains unaffected by the addition of the ethynyl phenyl groups. Overall, this gives a S···S distance of 32.0 Å.

Cyclic Voltammetry. Cyclic voltammograms were recorded for mononuclear $[2][PF_6]_2$ in 0.1 M $TBAPF_6$ in acetonitrile and referenced against ferrocene (i.e., $E_{1/2}$ $FeCp_2/[FeCp_2]^+$ = 0.00 V). The response of $[1][PF_6]_2$ under the same conditions has been described earlier.[34] These complexes each exhibit a single oxidation wave at 0.87 ($[1][PF_6]_2$) and 1.06 V ($[2][PF_6]_2$), assumed to be primarily metal-based (Ru(II)/Ru(III)).[51] A single broad reduction wave at −1.49 V was also observed for $[2][PF_6]_2$ (Table 1). The peak-to-peak separation (ΔE_p) of the oxidation wave in $[2][PF_6]_2$ (93 mV) compares with that of the internal ferrocene couple (82 mV). However, the significant increase in ΔEp associated with the reduction process (179 mV) suggests that this feature may be associated with two redox events in close succession, which is entirely consistent with the sequential reduction of the tpy ligands in $[1][PF_6]_2$ (Table 1). A second chemically irreversible oxidation event was observed near 1.08 V for $[1][PF_6]_2$ and 1.22 V for $[2][PF_6]_2$. On the basis of irreversible oxidations observed for L^1 and L^2 between 1.1−1.2 V these irreversible processes in the complexes can be attributed to the oxidation of the thiomethyl fragment.

The electrochemical response of bimetallic $\{L_nRu^{II}\}(\mu\text{-tpp})\{Ru^{II}L_n\}$ complexes have been studied extensively, giving rise to Robin−Day class III mixed-valent complexes, or radical cations with a noninnocent bridging phenazine ring, on one-electron oxidation.[31,54] As with similar complexes, the voltammogram of both $[3][PF_6]_4$ and $[4][PF_6]_4$ in acetonitrile (0.1 M NBu_4PF_6) display two one-electron oxidation waves attributed to the (formally) Ru(II,II)/Ru(II,III) and Ru(II,III)/Ru(III,III) redox couples (0.76 and 1.27 V for $[3][PF_6]_4$, and 0.90 and 1.39 V for $[4][PF_6]_4$)[55] (Figure 4, Table 1), although the tpp ligand is almost certainly redox noninnocent. A third

DOI: 10.1021/acs.inorgchem.5b00507
Inorg. Chem. 2015, 54, 5487−5494

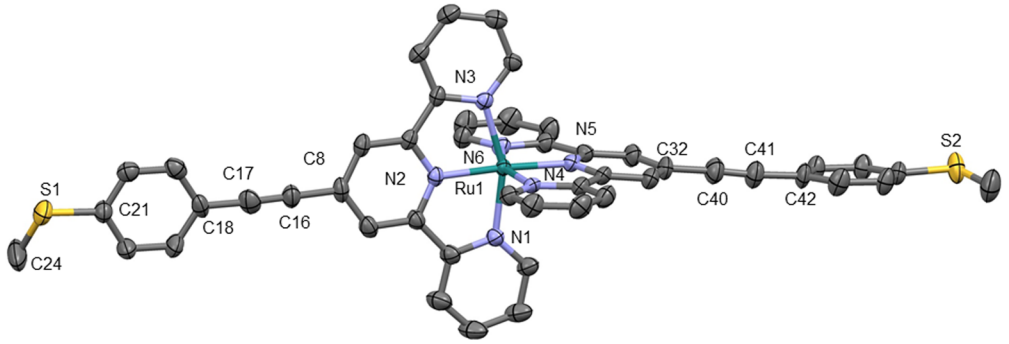

Figure 2. A plot of the cation in the crystal structure of $[\mathbf{2}][PF_6]2{\cdot}CH_3CN$, with hydrogen atoms omitted for clarity. Thermal ellipsoids are plotted at 50%.

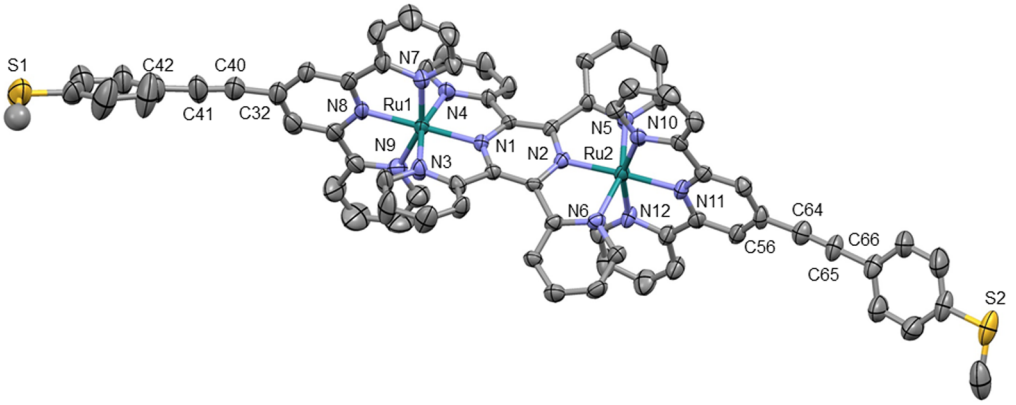

Figure 3. A plot of the cation in the crystal structure of $[\mathbf{4}][PF_6]_4{\cdot}3CH_3CN$, with hydrogen atoms removed for clarity. Thermal ellipsoids are plotted at 50%.

Table 1. Electrochemical Data for Compounds $[\mathbf{1}][PF_6]_2$, $[\mathbf{2}][PF_6]_2$, $[\mathbf{3}][PF_6]_4$, and $[\mathbf{4}][PF_6]_4$, Recorded in Acetonitrile 1.0 M $TBAPF_6$

	$E_{1/2}$ ($V_{Fc/Fc+}$) (ΔE_p[a] (mV))							
compound	SMe/SMe^+	Ru^{II}/Ru^{III}	Ru^{II}/Ru^{III}	$tpp/tpp^{\bullet-}$	$tpp^{\bullet-}/tpp^{2-}$	$tpy/tpy^{\bullet-}$	$tpy^{\bullet-}/tpy^{2-}$	$\Delta E_{1/2}$(ox)
$[\mathbf{1}][PF_6]_2$	1.08(nap)		0.87 (83)			−1.62 (95)	−1.92 (100)	
$[\mathbf{2}][PF_6]_2$	1.22(nap)		1.06 (93)			−1.49 (179)		
$[\mathbf{3}][PF_6]_4$	1.88(204)	1.27 (84)	0.76 (93)	−1.13 (nap)				510
$[\mathbf{4}][PF_6]_4$	1.93 (155)	1.39 (106)	0.90 (85)	−0.90 (85)	−1.20 (80)			490
$[\{(tpy)Ru\}(\mu\text{-tpp})\{Ru(tpy)\}][PF_6]_4$[31]		1.35 (85)	1.03 (75)	−0.76 (60)	−1.25 (60)	−1.83 (115)		320

[a]Peak-to-peak separation (ΔE_p) is shown in brackets. nap = no anodic peak observed.

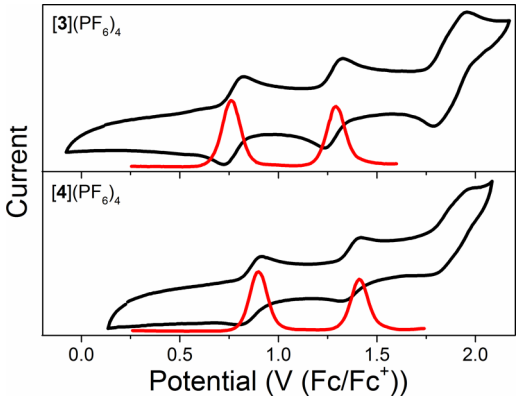

Figure 4. Plots of the CV of $[\mathbf{3}][PF_6]_4$ and $[\mathbf{4}][PF_6]_4$, showing the oxidation waves recorded in acetonitrile 1.0 M $TBAPF_6$ at a scan rate of 100 mV s^{-1}.

irreversible oxidation event at 1.88 V ($[\mathbf{3}][PF_6]_4$) and 1.93 V ($[\mathbf{4}][PF_6]_4$) is also observed and attributed to the oxidation of the thiomethyl groups. The potential for the first oxidation of $[\mathbf{4}][PF_6]_4$ is 140 mV more positive than that of $[\mathbf{3}][PF_6]_4$, a consequence of the presence of the electron-withdrawing alkyne moiety, as was observed for $[\mathbf{1}][PF_6]_2$ and $[\mathbf{2}][PF_6]_2$. A similar shift (120 mV) is apparent when the second oxidation potentials are compared, suggesting that the redox properties are not solely localized to the Ru-tpp-Ru cores. The large separation of the two oxidation events points to the significant thermodynamic stability of the formally Ru(II,III) mixed-valence state with respect to disproportionation. Finally, $[\mathbf{3}][PF_6]_4$ has a reduction at −1.13 V that is not chemically reversible, while $[\mathbf{4}][PF_6]_4$ shows two reversible reductions at −0.90 and −1.20 V; on the basis of similar complexes reported these are attributed to the reduction of tpp, since the tpy reduction is not visible within the electrochemical window.

DOI: 10.1021/acs.inorgchem.5b00507
Inorg. Chem. 2015, 54, 5487−5494

On the basis of the onset potentials of the first oxidation and reduction for the compounds $[1][PF_6]_2$–$[4][PF_6]_4$ the highest occupied molecular orbital (HOMO) and lowest unoccupied molecular orbital (LUMO) energy levels were determined, using $FeCp_2$ HOMO = −4.8 eV (Table 2).[56] Each of the

Table 2. HOMO and LUMO Energy Levels for Compounds $[1][PF_6]_2$–$[4][PF_6]_4$ Calculated from the Onset Potentials of the First Oxidation and Reduction for the Compounds

compound	HOMO (eV)	LUMO (eV)
$[1][PF_6]_2$	−5.67	−3.28
$[2][PF_6]_2$	−5.85	−3.46
$[3][PF_6]_4$	−5.55	−3.96
$[4][PF_6]_4$	−5.68	−4.06

complexes has a HOMO energy between −5.55 and −5.85 eV, which is relatively close to the work function of clean gold (5.1−5.3 eV). The LUMO energy levels are −3.28 to −4.06 eV, which is significantly lower than the work function of clean gold. This could indicate that HOMO-type conductance may be favored for these molecules.

Molecular Conductance. The single-molecule conductance of compounds $[1][PF_6]_2$, $[2][PF_6]_2$, $[3][PF_6]_4$, and $[4][PF_6]_4$ was determined using the STM $I(s)$ method,[36] as described in the Experimental Section with gold substrates in 1,2,4-trichlorobenzene solution and electrochemically etched gold STM tips. A bias voltage of 0.6 V and set point current of 30 nA were employed for $[1][PF_6]_2$, $[2][PF_6]_2$, and $[3][PF_6]_4$ and 10 nA for $[4][PF_6]_4$. To record current-distance traces the STM tip was brought close to the Au surface with the applied set point parameters, and then the tip was withdrawn at a speed of 40 nm/s, and the current-distance ($I(s)$) relation was logged. This process was repeated continuously, and 526, 375, 548, and 290 scans were collected showing characteristic plateaus for $[1][PF_6]_2$, $[2][PF_6]_2$, $[3][PF_6]_4$, and $[4][PF_6]_4$, respectively.

The conductance values, 95th percentile break-off distances, and calculated molecular lengths are summarized in Table 3,

Table 3. Conductance and Break-off Distance Values for $[1][PF_6]_2$, $[2][PF_6]_2$, $[3][PF_6]_4$, and $[4][PF_6]_4$

		Measured break-off distances and molecular lengths either obtained from X-ray structures or molecular modeling. All distances in nm.		
molecule	conductance (nS)	measured 95th percentile maximum break-off distance[a]	X-ray	molecular model
$[1][PF_6]_2$	2.1	1.9	2.15	2.17
$[2][PF_6]_2$	1.3	1.8	2.65	2.68
$[3][PF_6]_4$	0.78	2.4		2.84
$[4][PF_6]_4$	0.43	2.1	3.20	3.35

[a]95th percentile break-off distance observed across the collected $I(s)$ scans. Molecular length determined by X-ray analysis and DFT molecular modelling (B3LYP, LANL2DZ/6-31G(d)) are also shown.

with conductance histograms shown in Figure 5, while representative conductance traces showing current plateaus as well as two-dimensional histograms are given in the Supporting Information. Note that break-off distances are typically shorter than the length of a fully extended molecular junction. This is consistent with the molecules not being fully extended into a vertical configuration in the gold-molecule-gold junction due to the details of the molecule−surface contact, as well as the

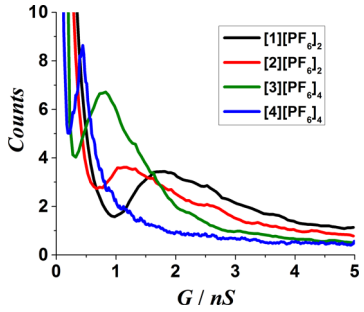

Figure 5. Normalized conductance histograms for the molecular targets.

stochastic nature of the junction breaking process. In this respect, important points to note about the thiomethyl group are its weaker adsorption to gold than the thiolate group and also a degree of steric hindrance provided by the terminal methyl groups, which may prevent formation of fully upright configuration for many junction arrangements. It is therefore not surprising that the break-off length falls short of the fully extended junction configuration.

To appreciate the decay of conductance with molecular length across this series of molecules, Figure 6 plots

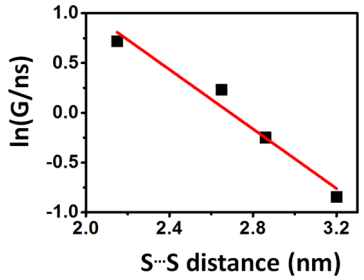

Figure 6. Plot of ln(G/nS) vs S···S distance (nm).

ln(conductance) versus S···S distance. The conductance is seen to fall off approximately exponentially with molecule length, following the relationship $G \propto e^{-\beta L}$, where G is the conductance, L is the length of the molecular bridge, and β is the tunnelling decay factor. Although the slope of the plot informs about the conductance attenuation with length across this series, it is not strictly a true β-factor since this group of molecules does not represent a homologous series in which length is increased by adding repeating moieties (such as methylene groups in an alkanedithiol homologous series). Nevertheless, the length dependence of the conductance is an interesting factor in benchmarking conductance across this series of related molecules. The slope of the ln G versus length plot ("decay factor", β) shown in Figure 6 is 1.5 nm^{-1}. It is instructive to compare this value with other β-values for conjugated aromatic rodlike molecular wires measured in the tunnelling charge transport regime. In the case of oligo(phenylene-ethynylene) molecular wires (OPEs) a β factor of 2.1 nm^{-1} was obtained by Liu et al. with thiolate termini,[57] while Kaliginedi et al. obtained β = 3.4 nm^{-1}.[5] Lu et al. obtained a β factor of 2.0 nm^{-1} for a series of amine-terminated OPE molecular wires up to 2.75 nm long.[58] Larger decay factors of 4.0 nm^{-1} have been obtained for oligophenylenes. On the other hand smaller decay factors have been recorded for oligo-ynes (0.6 nm^{-1}),[2] oligo-thiophenes (1 nm^{-1}),[59] oligo-porphyrins (0.4 nm^{-1}),[60] and extended viologens (0.06

DOI: 10.1021/acs.inorgchem.5b00507
Inorg. Chem. 2015, 54, 5487−5494

nm^{-1}).[61] The decay factor across the series of molecules $[\mathbf{1}][PF_6]_2$ to $[\mathbf{4}][PF_6]_4$ lies in between decay factors for oligoynes and oligophenylenes, which aligns with our chemical perception of these molecules being less conjugated than the former but more conjugated than the latter. The linear dependence of ln(molecular conductance) versus molecular length and the comparative magnitude of the slope points to consistency with a tunnelling mechanism.

CONCLUSIONS

The combination of the terpyridine ligands $\mathbf{L^1}$, $\mathbf{L^2}$, and the bridging bis(terchelate) tpp gives the wirelike complexes $[\mathbf{1}]^{2+}$–$[\mathbf{4}]^{4+}$ with S···S distances spanning up to ∼3 nm. The pseudodecay constant extracted from the single-molecule conductance values against molecular length is comparable to related organic compounds bearing alkyne and phenylene moieties, with the linear dependence of ln(molecular conductance) versus molecular length and the magnitude of the slope consistent with a tunnelling mechanism.

ASSOCIATED CONTENT

Supporting Information

Crystallographic information files (CIF) for compounds $\mathbf{L^2}$, $[\mathbf{2}][PF_6]_2{\cdot}CH_3CN$, and $[\mathbf{4}][PF_6]_4{\cdot}3CH_3CN$. NMR spectra, selected bond parameters, CV plots, and $I(s)$ data.The Supporting Information is available free of charge on the ACS Publications website at DOI: 10.1021/acs.inorgchem.5b00507.

AUTHOR INFORMATION

Corresponding Author

*E-mail: paul.low@uwa.edu.au.

Notes

The authors declare no competing financial interest.

ACKNOWLEDGMENTS

We gratefully acknowledge the EPSRC (EP/K007785/1; EP/K007548/1) for funding this work. P.J.L. gratefully acknowledges support from the Australian Research Council (DP140100855) and the award of a Future Fellowship (FT120100073).

REFERENCES

(1) Sun, L.; Diaz-Fernandez, Y. A.; Gschneidtner, T. A.; Westerlund, F.; Lara-Avila, S.; Moth-Poulsen, K. *Chem. Soc. Rev.* **2014**, *43*, 7378–7411.
(2) Wang, C. S.; Batsanov, A. S.; Bryce, M. R.; Martin, S.; Nichols, R. J.; Higgins, S. J.; Garcia-Suarez, V. M.; Lambert, C. J. *J. Am. Chem. Soc.* **2009**, *131*, 15647–15654.
(3) Moreno-Garcia, P.; Gulcur, M.; Manrique, D. Z.; Pope, T.; Hong, W.; Kaliginedi, V.; Huang, C.; Batsanov, A. S.; Bryce, M. R.; Lambert, C.; Wandlowski, T. *J. Am. Chem. Soc.* **2013**, *135*, 12228–12240.
(4) Wold, D. J.; Haag, R.; Rampi, M. A.; Frisbie, C. D. *J. Phys. Chem. B* **2002**, *106*, 2813–2816.
(5) Kaliginedi, V.; Moreno-García, P.; Valkenier, H.; Hong, W.; García-Suárez, V. M.; Buiter, P.; Otten, J. L. H.; Hummelen, J. C.; Lambert, C. J.; Wandlowski, T. *J. Am. Chem. Soc.* **2012**, *134*, 5262–5275.
(6) Masai, H.; Terao, J.; Seki, S.; Nakashima, S.; Kiguchi, M.; Okoshi, K.; Fujihara, T.; Tsuji, Y. *J. Am. Chem. Soc.* **2014**, *136*, 1742–1745.
(7) Lissel, F.; Schwarz, F.; Blacque, O.; Riel, H.; Lörtscher, E.; Venkatesan, K.; Berke, H. *J. Am. Chem. Soc.* **2014**, *136*, 14560–14569.
(8) Schwarz, F.; Kastlunger, G.; Lissel, F.; Riel, H.; Venkatesan, K.; Berke, H.; Stadler, R.; Lörtscher, E. *Nano Lett.* **2014**, *14*, 5932–5940.
(9) Rigaut, S. *Dalton Trans.* **2013**, *42*, 15859–15863.
(10) Low, P. J. *Dalton Trans.* **2005**, 2821–2824.
(11) Albrecht, T.; Guckian, A.; Kuznetsov, A. M.; Vos, J. G.; Ulstrup, J. *J. Am. Chem. Soc.* **2006**, *128*, 17132–17138.
(12) Albrecht, T.; Moth-Poulsen, K.; Christensen, J. B.; Hjelm, J.; Bjørnholm, T.; Ulstrup, J. *J. Am. Chem. Soc.* **2006**, *128*, 6574–6575.
(13) Kastlunger, G.; Stadler, R. *Phys. Rev. B* **2013**, *88*, 035418–035428.
(14) Meng, F.; Hervault, Y.-M.; Shao, Q.; Hu, B.; Norel, L.; Rigaut, S.; Chen, X. *Nat. Commun.* **2014**, *5*, 3023–3032.
(15) Osorio, E. A.; Moth-Poulsen, K.; van der Zant, H. S. J.; Paaske, J.; Hedegård, P.; Flensberg, K.; Bendix, J.; Bjørnholm, T. *Nano Lett.* **2009**, *10*, 105–110.
(16) Nakamura, H.; Ohto, T.; Ishida, T.; Asai, Y. *J. Am. Chem. Soc.* **2013**, *135*, 16545–16552.
(17) Albrecht, T.; Moth-Poulsen, K.; Christensen, J. B.; Guckian, A.; Bjornholm, T.; Vos, J. G.; Ulstrup, J. *Faraday Discuss.* **2006**, *131*, 265–279.
(18) Tuccitto, N.; Ferri, V.; Cavazzini, M.; Quici, S.; Zhavnerko, G.; Licciardello, A.; Rampi, M. A. *Nat. Mater.* **2009**, *8*, 41–46.
(19) Wen, H.-M.; Yang, Y.; Zhou, X.-S.; Liu, J.-Y.; Zhang, D.-B.; Chen, Z.-B.; Wang, J.-Y.; Chen, Z.-N.; Tian, Z.-Q. *Chem. Sci.* **2013**, *4*, 2471–2477.
(20) Kobayashi, K.; Tonegawa, N.; Fujii, S.; Hikida, J.; Nozoye, H.; Tsutsui, K.; Wada, Y.; Chikira, M.; Haga, M.-a. *Langmuir* **2008**, *24*, 13203–13211.
(21) Terada, K.; Kobayashi, K.; Haga, M.-a. *Dalton Trans.* **2008**, 4846–4854.
(22) Sakamoto, R.; Katagiri, S.; Maeda, H.; Nishimori, Y.; Miyashita, S.; Nishihara, H. *J. Am. Chem. Soc.* **2015**, *137*, 734–741.
(23) Maeda, H.; Sakamoto, R.; Nishihara, H. *Chem.—Eur. J.* **2014**, *20*, 2761–2764.
(24) Sakamoto, R.; Ohirabaru, Y.; Matsuoka, R.; Maeda, H.; Katagiri, S.; Nishihara, H. *Chem. Commun.* **2013**, *49*, 7108–7110.
(25) Sakamoto, R.; Katagiri, S.; Maeda, H.; Nishihara, H. *Coord. Chem. Rev.* **2013**, *257*, 1493–1506.
(26) Ruben, M.; Landa, A.; Lörtscher, E.; Riel, H.; Mayor, M.; Görls, H.; Weber, H. B.; Arnold, A.; Evers, F. *Small* **2008**, *4*, 2229–2235.
(27) Ruminski, R. R.; Aasen, T. D. *Inorg. Chim. Acta* **2010**, *363*, 905–910.
(28) Padilla, R.; Ruminski, R. R.; Meredith McGinley, V. A.; Williams, P. B. *Polyhedron* **2012**, *33*, 158–165.
(29) Yao, C.-J.; Zheng, R.-H.; Nie, H.-J.; Cui, B.-B.; Shi, Q.; Yao, J.; Zhong, Y.-W. *Chem.—Eur. J.* **2013**, *19*, 12376–12387.
(30) Yao, C.-J.; Zhong, Y.-W.; Yao, J. *Inorg. Chem.* **2013**, *52*, 4040–4045.
(31) Wadman, S. H.; Havenith, R. W. A.; Hartl, F.; Lutz, M.; Spek, A. L.; van Klink, G. P. M.; van Koten, G. *Inorg. Chem.* **2009**, *48*, 5685–5696.
(32) Potts, K. T.; Konwar, D. *J. Org. Chem.* **1991**, *56*, 4815–4816.
(33) Huang, G.; Yang, C.; Xu, Z.; Wu, H.; Li, J.; Zeller, M.; Hunter, A. D.; Chui, S. S.-Y.; Che, C.-M. *Chem. Mater.* **2009**, *21*, 541–546.
(34) Constable, E. C.; Housecroft, C. E.; Medlycott, E.; Neuburger, M.; Reinders, F.; Reymann, S.; Schaffner, S. *Inorg. Chem. Commun.* **2008**, *11*, 518–520.
(35) Hartshorn, C. M.; Daire, N.; Tondreau, V.; Loeb, B.; Meyer, T. J.; White, P. S. *Inorg. Chem.* **1999**, *38*, 3200–3206.
(36) Haiss, W.; van Zalinge, H.; Higgins, S. J.; Bethell, D.; Höbenreich, H.; Schiffrin, D. J.; Nichols, R. J. *J. Am. Chem. Soc.* **2003**, *125*, 15294–15295.
(37) Haiss, W.; Nichols, R. J.; van Zalinge, H.; Higgins, S. J.; Bethell, D.; Schiffrin, D. J. *Phys. Chem. Chem. Phys.* **2004**, *6*, 4330–4337.
(38) Sheldrick, G. *Acta Crystallogr., Sect. A* **2008**, *64*, 112–122.
(39) Dolomanov, O. V.; Bourhis, L. J.; Gildea, R. J.; Howard, J. A. K.; Puschmann, H. *J. Appl. Crystallogr.* **2009**, *42*, 339–341.
(40) Frisch, M. J.; Trucks, G. W.; Schlegel, H. B.; Scuseria, G. E.; Robb, M. A.; Cheeseman, J. R.; Scalmani, G.; Barone, V.; Mennucci, B.; Petersson, G. A.; Nakatsuji, H.; Caricato, M.; Li, X.; Hratchian, H. P.; Izmaylov, A. F.; Bloino, J.; Zheng, G.; Sonnenberg, J. L.; Hada, M.;

DOI: 10.1021/acs.inorgchem.5b00507
Inorg. Chem. 2015, 54, 5487–5494

Ehara, M.; Toyota, K.; Fukuda, R.; Hasegawa, J.; Ishida, M.; Nakajima, T.; Honda, Y.; Kitao, O.; Nakai, H.; Vreven, T.; Montgomery, J. A., Jr.; Peralta, J. E.; Ogliaro, F.; Bearpark, M.; Heyd, J. J.; Brothers, E.; Kudin, K. N.; Staroverov, V. N.; Kobayashi, R.; Normand, J.; Raghavachari, K.; Rendell, A.; Burant, J. C.; Iyengar, S. S.; Tomasi, J.; Cossi, M.; Rega, N.; Millam, J. M.; Klene, M.; Knox, J. E.; Cross, J. B.; Bakken, V.; Adamo, C.; Jaramillo, J.; Gomperts, R.; Stratmann, R. E.; Yazyev, O.; Austin, A. J.; Cammi, R.; Pomelli, C.; Ochterski, J. W.; Martin, R. L.; Morokuma, K.; Zakrzewski, V. G.; Voth, G. A.; Salvador, P.; Dannenberg, J. J.; Dapprich, S.; Daniels, A. D.; Farkas, Ö.; Foresman, J. B.; Ortiz, J. V.; Cioslowski, J.; Fox, D. J. *Gaussian 09*, Version A.1; Gaussian, Inc: Wallingford, CT, 2009.

(41) Becke, A. D. *J. Chem. Phys.* **1993**, *98*, 5648−5652.

(42) Stephens, P. J.; Devlin, F. J.; Chabalowski, C. F.; Frisch, M. J. *J. Phys. Chem.* **1994**, *98*, 11623−11627.

(43) Hay, P. J.; Wadt, W. R. *J. Chem. Phys.* **1985**, *82*, 299−310.

(44) Petersson, G. A.; Al-Laham, M. A. *J. Chem. Phys.* **1991**, *94*, 6081−6090.

(45) Schönherr, H.; Kremer, F. J. B.; Kumar, S.; Rego, J. A.; Wolf, H.; Ringsdorf, H.; Jaschke, M.; Butt, H. J.; Bamberg, E. *J. Am. Chem. Soc.* **1996**, *118*, 13051−13057.

(46) Capozzi, B.; Dell, E. J.; Berkelbach, T. C.; Reichman, D. R.; Venkataraman, L.; Campos, L. M. *J. Am. Chem. Soc.* **2014**, *136*, 10486−10492.

(47) Wen, H.-M.; Zhang, D.-B.; Zhang, L.-Y.; Shi, L.-X.; Chen, Z.-N. *Eur. J. Inorg. Chem.* **2011**, *2011*, 1784−1791.

(48) Du, P.; Schneider, J.; Brennessel, W. W.; Eisenberg, R. *Inorg. Chem.* **2007**, *47*, 69−77.

(49) Graczyk, A.; Murphy, F. A.; Nolan, D.; Fernandez-Moreira, V.; Lundin, N. J.; Fitchett, C. M.; Draper, S. M. *Dalton Trans.* **2012**, *41*, 7746−7754.

(50) Lee, Y. H.; Nghia, N. V.; Go, M. J.; Lee, J.; Lee, S. U.; Lee, M. H. *Organometallics* **2014**, *33*, 753−762.

(51) Maestri, M.; Armaroli, N.; Balzani, V.; Constable, E. C.; Thompson, A. C. *Inorg. Chem.* **1995**, *34*, 2759−2767.

(52) Lashgari, K.; Kritikos, M.; Norrestam, R.; Norrby, T. *Acta Crystallogr., Sect. C: Cryst. Struct. Commun.* **1999**, *55*, 64−67.

(53) Yoshikawa, N.; Yamabe, S.; Kanehisa, N.; Inoue, T.; Takashima, H.; Tsukahara, K. *J. Phys. Org. Chem.* **2011**, *24*, 1110−1118.

(54) Ghumaan, S.; Sarkar, B.; Chanda, N.; Sieger, M.; Fiedler, J.; Kaim, W.; Lahiri, G. K. *Inorg. Chem.* **2006**, *45*, 7955−7961.

(55) Wadman, S. H.; Lutz, M.; Tooke, D. M.; Spek, A. L.; Hartl, F.; Havenith, R. W. A.; van Klink, G. P. M.; van Koten, G. *Inorg. Chem.* **2009**, *48*, 1887−1900.

(56) Ahmida, M. M.; Eichhorn, S. H. *ECS Trans.* **2010**, *25*, 1−10.

(57) Liu, K.; Li, G.; Wang, X.; Wang, F. *J. Phys. Chem. C* **2008**, *112*, 4342−4349.

(58) Lu, Q.; Liu, K.; Zhang, H.; Du, Z.; Wang, X.; Wang, F. *ACS Nano* **2009**, *3*, 3861−3868.

(59) Yamada, R.; Kumazawa, H.; Noutoshi, T.; Tanaka, S.; Tada, H. *Nano Lett.* **2008**, *8*, 1237−1240.

(60) Sedghi, G.; Sawada, K.; Esdaile, L. J.; Hoffmann, M.; Anderson, H. L.; Bethell, D.; Haiss, W.; Higgins, S. J.; Nichols, R. J. *J. Am. Chem. Soc.* **2008**, *130*, 8582−8583.

(61) Kolivoška, V.; Valášek, M.; Gál, M.; Sokolová, R.; Bulíčková, J.; Pospíšil, L.; Mészáros, G.; Hromadová, M. *J. Phys. Chem. Lett.* **2013**, *4*, 589−595.

DOI: 10.1021/acs.inorgchem.5b00507
Inorg. Chem. 2015, 54, 5487−5494